Modelling roughness effects for transitional low Reynolds number aerofoil flows

Article *in* Proceedings of the Institution of Mechanical Engineers Part G Journal of Aerospace Engineering · January 2014

DOI: 10.1177/0954410014530875

2 authors:

Sheng Liu
Kuang-Chi Institute of Advanced Technology
1 PUBLICATION **4** CITATIONS
SEE PROFILE

Ning Qin
The University of Sheffield
247 PUBLICATIONS **2,657** CITATIONS
SEE PROFILE

Original Article

Institution of MECHANICAL ENGINEERS
Journal of AEROSPACE ENGINEERING

Proc IMechE Part G:
J Aerospace Engineering
2015, Vol. 229(2) 280–289

DOI: 10.1177/0954410014530875
uk.sagepub.com/jaero
SAGE

Modelling roughness effects for transitional low Reynolds number aerofoil flows

S Liu and N Qin

Abstract

Roughness modelling at low Reynolds numbers of O(10^4–10^5) is of practical importance for micro air vehicles. This paper investigates the roughness modelling behaviour of the low Reynolds number shear stress transport model and the γ-Re_θ shear stress transport model. Both include modelling flow transition and surface roughness effects. The roughness effects are modelled as sand grain roughness. A series of simulations using the two models have been performed on a NACA0012 aerofoil with comparisons to available experimental data. The results show that both of the models have the capability to reasonably predict the leading edge laminar separation bubble, transition and skin friction and, therefore, lift and drag on smooth surfaces. However, the two models behave very differently for the rough surface aerofoil. While the low Reynolds number shear stress transport model performs well, the γ-Re_θ model fails to predict the transition on the rough aerofoil surface, resulting in inaccurate lift and drag prediction.

Keywords

Low Reynolds number, roughness effects, transition modelling, micro air vehicles, computational fluid dynamics

Date received: 27 September 2013; accepted: 14 March 2014

Introduction

Micro air vehicles (MAVs) operate at low Reynolds numbers, in the order of O(10^4–10^5). Similar to higher Reynolds number aircraft, surface roughness can have a significant effect on the vehicle aerodynamics. Considerable experimental investigation on roughness effects at low Reynolds numbers has been conducted for applications of model airplanes. Schmitz[1] proposed 'artificial turbulence' to improve the aerodynamic performance, including surface roughness. Kraemer[2] continued from the idea of Schmitz, and the investigation on the Gö 801 aerofoil with rough paper covering showed better lift and drag characteristics below the Reynolds number of 7.5×10^4. Lyon et al.[3] reported drag reduction in the experiments of SD7037 and RG15 aerofoils with rough fibre glass weave and rough wood-grain finish. Althaus[4] also provided valuable aerofoil data with surface roughness from normal constructions. Simons[5] later made a qualitative conclusion on surface roughness, stating that roughness can be useful to deal with the 'subcritical problem' and otherwise maintaining accurate shape is of importance. The benefit of surface roughness usually can be attributed to its effects on the laminar separation bubble. Surface roughness can promote boundary layer transition and reduce form drag as the separation bubble can be reduced or eliminated. Accurate modelling of such effects is therefore of practical value.

The type of roughness may be categorised as single/isolated roughness and distributed roughness. The study of the former usually investigates the critical height of roughness elements to trigger boundary layer transition, and considerable knowledge and experience has been accumulated, such as the trip wire roughness for low Reynolds number flows by Gopalarathnam et al.[6] Recently, Zhou and Wang[7] conducted a computational work on roughness bumps that can be seen as an analogy to trip wires, reporting that the lift to drag ratio of an SD7003 aerofoil was improved by 29% when $Re = 6 \times 10^4$. For this type of single element roughness, the exact

Department of Mechanical Engineering, University of Sheffield, Sheffield, UK

Corresponding author:
N Qin, Department of Mechanical Engineering, University of Sheffield, Mappin Street, Sheffield, S1 3JD, UK.
Email: n.qin@sheffield.ac.uk

roughness geometrical description is retained in the numerical simulations.

The distributed roughness is relatively more complicated that the detailed description of the roughness geometry is usually not retained in simulations due to geometric complexity. This type of roughness is closer to real life rough surfaces, and its shape and density can differ from surface to surface. One approach is to model the exact geometry. Huebsch et al.[8] simulated the effects of a dynamic roughness strip, preserving the roughness geometries in the modelling, however, leading to expensive computations because a large number of computational cells are required.

A more efficient approach is to treat this type of roughness as equivalent sand grains. The method is based on Nikuradse's early rough pipe experiments,[9] from which the universal law-of-wall for rough walls was proposed. By embedding this into the near wall treatment in turbulence modelling, roughness effects can then be simulated, e.g. Eça and Hoekstra.[10] Meanwhile, through certain correlations in the shape and density of roughness elements to Nikuradse's sand grains, real life roughness can eventually be simulated to some degree, such as Dirling's correlation.[11]

The universal law-of-the-wall for rough walls deals with turbulent boundary layers. Roughness-induced transition modelling needs to be considered for transitional flows. This can be realised through either low Reynolds number correction for a particular turbulence model, or through a correlation-based model. The early experimental work by Feindt[12] has been widely used to devise these approaches. Recently, Stripf et al.[13] developed new correlations and extensions to two turbulence models, and Elsner and Warzecha[14] implemented the correlations into the γ-Re_θ shear stress transport (SST) model. The correlation requires the information of the ratio between the roughness height and the boundary layer displacement thickness. However, the transition onset location prediction was not satisfactory. Dassler et al.[15] developed an approach to avoid this requirement by including additional transport equation of an amplification roughness variable for k-ω model.

The primary purpose of this paper is to assess the performance of two versions of the SST model on roughness modelling for MAV applications. To resolve the above mentioned flow features, the SST model with low Reynolds number correction and the γ-Re_θ model are considered. Our previous work[16] investigated the modelling of laminar separation bubbles using the γ-Re_θ SST model on smooth surfaces, showing reasonably accurate lift and drag prediction as compared to the experiment data.

Description of the referred experiment

This work compares the results from the two models with the experimental data by Chakroun et al.[17] The tested aerofoil is the NACA0012 aerofoil. The lift and drag coefficients data were measured between $-16^\circ \leqslant \alpha \leqslant 26^\circ$ on a smooth surface, surfaces with either P80 (200 μm) or Grit-36 (500 μm) sandpapers at $Re = 1.5 \times 10^5$. These data are compared to assess the overall performance of the two models. To further understand the difference between the two models on the prediction of laminar to turbulent transition, skin friction data are compared. The experiment collected corresponding data between Reynolds number 1.97×10^4 and 7.87×10^4, instead of specifying a clear number. In the simulations, a Reynolds number of 5×10^4 is assumed.

The freestream turbulence intensity was not clearly reported. The same researchers' previous work[18] reported the turbulence intensity less than 0.5% for the same wind tunnel. A value of 0.33% is chosen in the present simulations. Table 1 shows the freestream condition used in the simulation. There is some decay for the turbulence intensity from the flow inlet to the aerofoil leading edge. To maintain the prescribed value (0.33%), the input at the flow inlet is adjusted to 0.4% for the low Re SST model and 0.43% for the γ-Re_θ SST model.

The Grit-36 case is considered here. The nominal 500 μm was 'roughness thickness' mentioned in the experiment, which can be seen as the geometrical roughness height.

The equivalent sand grain roughness height is difficult to obtain. Ferrer and Munduate[19] estimated a relationship of $h_s/h = 2.043$ for a Grit-40 surface, and Pailhas et al.[20] reported an averaged value of $h_s/h = 2$ based on their experiment for a 3MP40 surface. Considering Grit-36 surface is close to the Grit-40 surface in grade, $h_s/h = 2$ or $h_s = 1000$ μm is assumed in the following simulations. Ideally, a dedicated experiment should be performed to identify the appropriate height.

The nondimensional roughness height h_s^+ is shown in Figure 1, calculated after the flow is solved. The h_s^+ values indicate this roughness height is in the transitional rough region for the $Re = 5 \times 10^4$ case and only the leading edge part is in the fully rough region for the $Re = 1.5 \times 10^5$ case. See section 'Rough wall

Table 1. Freestream properties.

$(\mu_t/\mu)_{inlet}$	*Tu* (%)	*T* (K)	Reynolds number	Mach number
10	0.33	293.15 (μ = 1.81 e-5 Pa·s)	150,000 or 50,000	0.0432 or 0.0144

boundary conditions' for the definition of transition rough and fully rough regions.

Numerical modelling

Flow solver

The flow is modelled numerically by solving steady-state compressible Reynolds-averaged Navier–Stokes (RANS) equations using the finite volume method. ANSYS FLUENT v14.0 is used in this study. The pressure-based coupled solver is chosen, because in practice it is found to be more robust and converging better than the segregated solvers in the low Reynolds number cases. The spatial discretisation is second-order upwind. Residuals in each governing equation and the lift and drag coefficient histories are monitored. The iterative convergence is checked when the variation of lift and drag coefficient drops below 10^{-4} within 100 iterations. In separation bubble-related cases, the bubble location remains steady when more iterations are performed, indicating that the flow field is sufficiently converged.

Turbulence models

Low Re SST model. The low Reynolds number SST (low Re SST) model is an extension of the original SST model.[21] The low Reynolds number SST model used in this paper is based on the updated SST model described by Menter et al.[22] The general idea for low Re correction is to activate damping function on the turbulent viscosity. The formulation follows similarly to the low Reynolds number version of the standard k-ω model. The low Re correction is made on the coefficient α^* when calculating the eddy viscosity, as follows

$$\mu_t = \frac{\rho k}{\omega} \frac{1}{\max[\frac{1}{\alpha^*}, \frac{SF_2}{\alpha_1 \omega}]} \tag{1}$$

where S is the strain rate magnitude, F_2 is the blending function defined in Menter et al.,[22] α_1 is one of the model constant with a value 0.31.

The coefficient α^* is calculated from[23]

$$\alpha^* = \alpha^*_\infty \left(\frac{\alpha^*_0 + Re_t/R_k}{1 + Re_t/R_k} \right) \tag{2}$$

with $Re_t = \rho k/\mu\omega$ and $R_k = 6$, $\alpha^*_0 = 0.024$, $\alpha^*_\infty = 1$.

γ-Re$_\theta$ SST model. The γ-Re$_\theta$ shear stress transport (γ-Re$_\theta$ SST) model[24] is a local correlation based transition model, which solves the transport equations for the intermittency factor and the transition momentum thickness Reynolds number, in addition to the standard SST model. The general idea is to localise the traditional empirical onset criteria via the vorticity Reynolds number, and then using intermittency factor to correct the turbulence productions. Several correlations are required to complete the formulation. The one used on smooth surfaces was published as the Langtry–Menter correlation.[24]

When roughness is simulated, the model uses an empirical correlation. It corrects the local transition momentum thickness, i.e. $\tilde{Re}_{\theta t,rough} = f(\tilde{Re}_{\theta t,smooth}, h_g)$, relying on the geometrical roughness height rather than the equivalent sand grain height, and then the obtained $\tilde{Re}_{\theta t,rough}$ is used to calculate the new critical Reynolds number and the

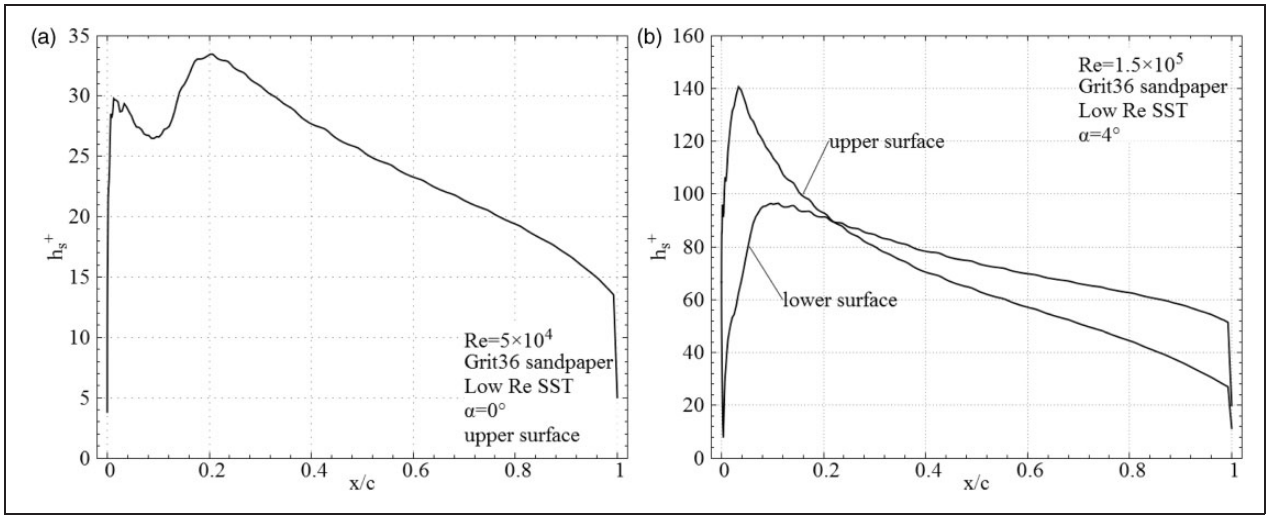

Figure 1. h_s^+ distribution.
SST: shear stress transport.

transition length function.[23] According to Langtry and Menter,[25] it is improved from the correlation by Mayle[26] and validated against Pimenta's flat plat data[27] and Karlsruhe's roughened turbine blade data.[28] However, the validations for low Reynolds number external flow with low freestream turbulence intensities are not available.

Two more points are discussed here for the two models. First, it is known that the high Reynolds number SST model tends to underestimate the skin friction, especially in fully rough cases, and an additional blending function by Hellsten and Laine[29] is required. The two models used in this work have no such blending function. To investigate the consequence, a user-defined function is written and then implemented into the low Re SST model in the software. The results show 0.9% drag coefficient increase at $\alpha = 0^\circ$ when $Re = 5 \times 10^4$ and $\alpha = 4^\circ$ when $Re = 1.5 \times 10^5$. Skin friction coefficients also show no significant change. Second, because the two models simulate laminar to turbulent transition distinctly, the normalised Reynolds shear stress with a threshold of 0.1% is adopted to compare the transition prediction. It is calculated via Boussinesq approximation, which is commonly used for eddy viscosity turbulence models, as follows

$$\tau_{xy} = -\rho u' \bar{v}' = \mu_t \left(\frac{\partial u}{\partial y} + \frac{\partial v}{\partial x} \right) \tag{3}$$

Rough wall boundary conditions

An automatic wall treatment[30] is used to model roughness effects via the ω boundary condition, which optimally blends the wall value of ω in the viscous sublayer and the log layer based on the near wall grid density. On smooth surfaces, it behaves like this, when the first layer height is sufficiently small, e.g. O(1) or less, the friction velocity u_τ and ω are determined from the sublayer formulation. In the case of roughness, according to Langtry and Menter,[25] the blending of sublayer and log layer value is not physically sensible when the sublayer is greatly disturbed, such as the fully rough cases. To overcome this deficiency, as well as to account for the blockage effects of the sand grain roughness, the cell wall distance is shifted by half of the roughness height, i.e. $y_{rough} = y + 0.5 h_s$. In this way, u_τ and ω wall values will primarily be determined from their log law formulations when the roughness height is much greater than the first layer height. The law of the wall for rough walls used is briefly described as follows, according to Ioselevich and Pilipenko[31]

$$u^+ = \frac{1}{\kappa} \ln y^+ + B - \Delta B \tag{4}$$

and the downshift ΔB is formulated as follows:

1. $h_s^+ \leqslant 2.25$, the hydraulically smooth, $\Delta B = 0$
2. $2.25 < h_s^+ \leqslant 90$, the transitional region, $\Delta B = \frac{1}{\kappa} \ln\left(\frac{h_s^+ - 2.25}{87.75} + C_s h_s^+ \right) \times \sin\left[0.4258 \left(\ln h_s^+ - 0.811 \right) \right]$
3. $h_s^+ > 90$, the fully rough region, $\Delta B = \frac{1}{\kappa} \ln\left(1 + C_s h_s^+ \right)$

where C_s is the roughness constant ($= 0.5$ for uniform sand grain surface), κ is the von Karman's constant (≈ 0.42).

Grid convergence

Figure 2(a) shows the geometry of computational domain and the boundary conditions. The far-field boundary is 20 chords away from the aerofoil. A sensitivity study of the far-field boundary location performed by the authors showed this size is appropriate.

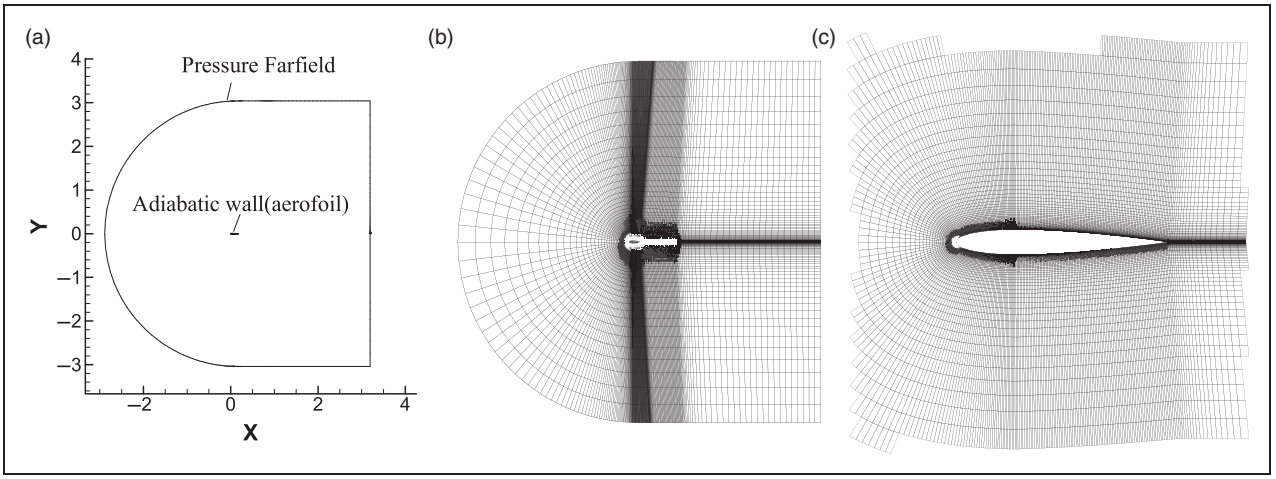

Figure 2. (a) Domain and boundary condition, (b) C-type grid, (c) grid elements near the aerofoil.

The computational grid is generated using ICEM grid generation program. The grid topology is a C-type. Further block splitting is made near the aerofoil to better control the boundary layer mesh and the mesh in the near wake. A base grid is generated at first and then refined or coarsened by a ratio of 1.5 along each axis to check grid convergence. The base grid has a maximum first grid layer's y^+ of approximately 0.7 ($Re = 1.5 \times 10^5$), (checked after the flow is solved), and a near-wall grid expansion ratio of 1.1, chosen according to the suggestion by Menter.[32]

The lift and drag coefficients at $\alpha = 4^\circ$ are compared, as shown in Table 2, with the grid convergence index (GCI) by Roache[33] shown in Table 3. The results show no convergence on drag coefficients in all cases, and no convergence on lift coefficients for the rough case using the γ-Re_θ SST model. The converged cases show super-convergence (the observed order of convergence is much greater than theoretical 2), and a value of 2 is adopted when calculating GCI. All available GCI values are in a satisfactory range.

Result and discussion

Lift and drag comparison at $Re = 1.5 \times 10^5$

The lift and drag coefficients are compared with available experimental data to evaluate the overall performance of the two models. The experiment data shows generally lower lift and higher drag for the Grit-36 case, when comparing to the results on smooth surfaces. The experimental observation therefore shows that the roughness deteriorated the aerofoil's lift and drag characteristics.

The lift and drag coefficients on smooth and rough surfaces predicted by the two models are presented in Figure 3 and Figure 4. On smooth surfaces, there is little difference on the lift and drag coefficients between the two models, and both lift and drag results before stall are in reasonably good agreement with the experiment.

On rough surfaces, the two models behave rather differently. The γ-Re_θ SST clearly overpredicts the lift and underpredicts the drag. On the other hand, the low Re SST model managed to predict the correct trend of the roughness effects, i.e. a decrease in lift coefficients and an increase in drag coefficients. The lift coefficient by the low Re SST compares well with the experimental data but the drag coefficient underpredicts the experimental data although upward trend from smooth surface drag is correct.

Skin friction result at $Re = 5 \times 10^4$

Figure 5(a) shows the skin friction predicted by the two models on smooth surfaces, comparing with the experimental data at $\alpha = 0^\circ$. On the smooth surface, the prediction by the two models agrees with the experiment very well, and the difference between the two models is below 0.1%. It is not surprising that the two models are consistently accurate at this laminar boundary layer condition as the eddy viscosities are negligible.

Figure 5(b) shows the results on the rough surfaces. It is observed that roughness-induced transition, as observed in the experiment, is predicted by the low Re SST model, while the γ-Re_θ SST clearly misses the transition on the rough aerofoil surface.

The drag coefficient results are compared to investigate the overall effect, as presented in Table 4. When the roughness is introduced, the low Re SST shows a 150% increase in the skin friction drag C_{df}, due to a transitional boundary layer. By comparison, the γ-Re_θ SST model shows only 2% increase, due to its failure in capturing transition on the rough surface. Although a reduction in the pressure drag C_{dp} is observed from the low Re SST results, it is overshadowed by the increase in the skin friction and the total drag C_d increases as a result. The decrease in pressure drag in the low Re SST result can be attributed to the reduction of the trailing edge

Table 3. Grid convergence index results for Grid 2.

	Smooth		Rough
	Low Re SST	γ-Re_θ SST	Low Re SST
$GCI_{fine,123}$ C_l	2.90%	1.50%	2.19%
P_{123} Cl	2.78	3.68	0.62

Table 2. Grid sensitivity results.

	Smooth				Rough			
	Low Re SST		γ-Re_θ SST		Low Re SST		γ-Re_θ SST	
Grid elements	C_l	C_d	C_l	C_d	C_l	C_d	C_l	C_d
Grid 3: 25706	0.4966	0.01314	0.5110	0.01410	0.3644	0.03216	0.4540	0.01057
Grid 2: 57312	0.4907	0.01315	0.5078	0.01402	0.3652	0.03235	0.4520	0.01075
Grid 1: 129102	0.4888	0.01295	0.5071	0.01387	0.3658	0.03235	0.4559	0.01044

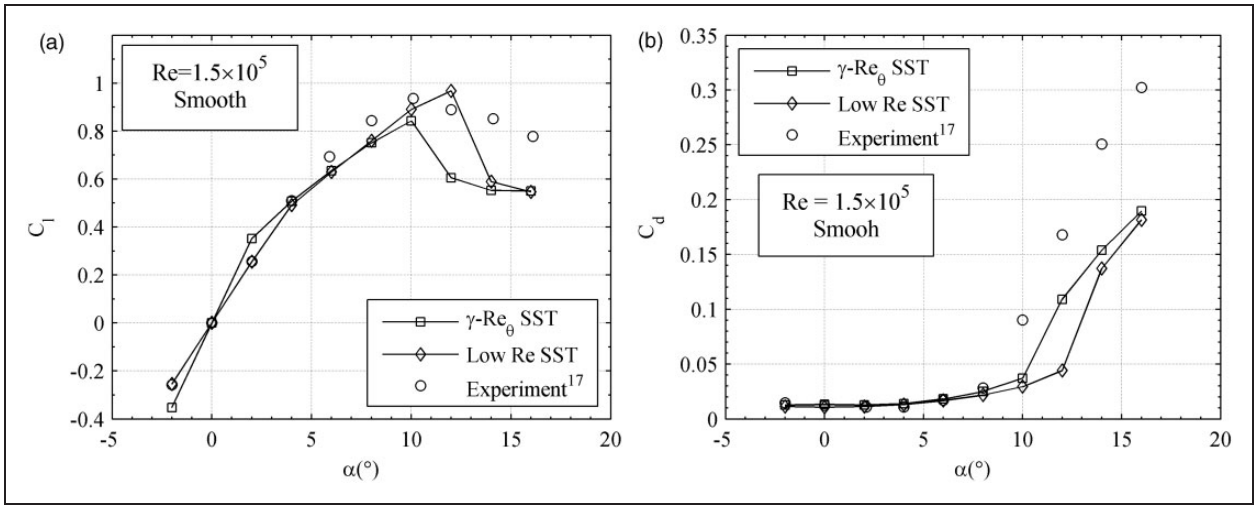

Figure 3. Lift and drag coefficients obtained on smooth surfaces.
SST: shear stress transport.

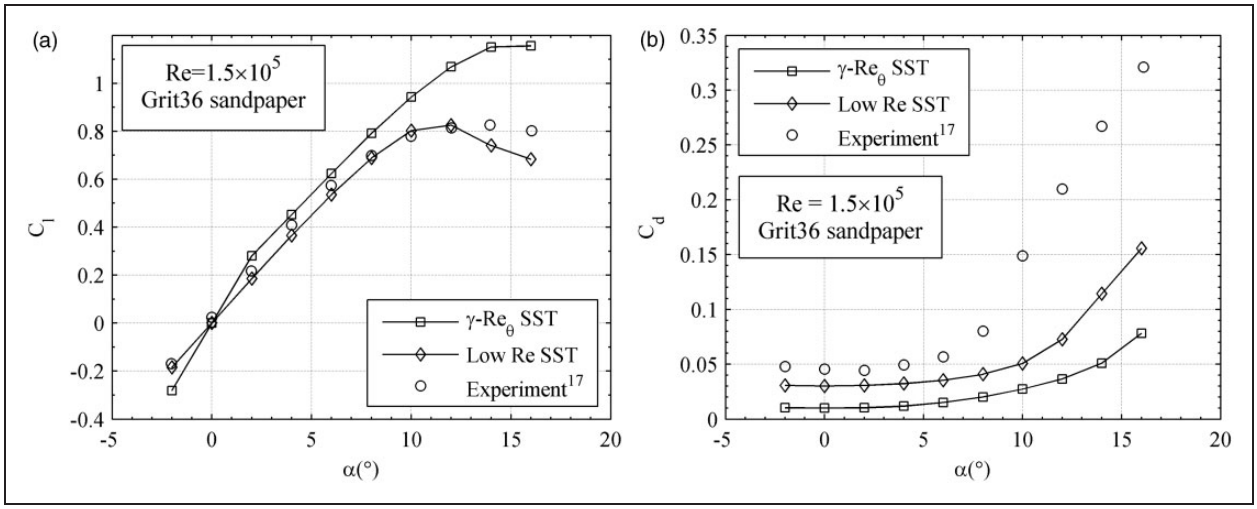

Figure 4. Lift and drag coefficients obtained on the Grit-36 surface.
SST: shear stress transport.

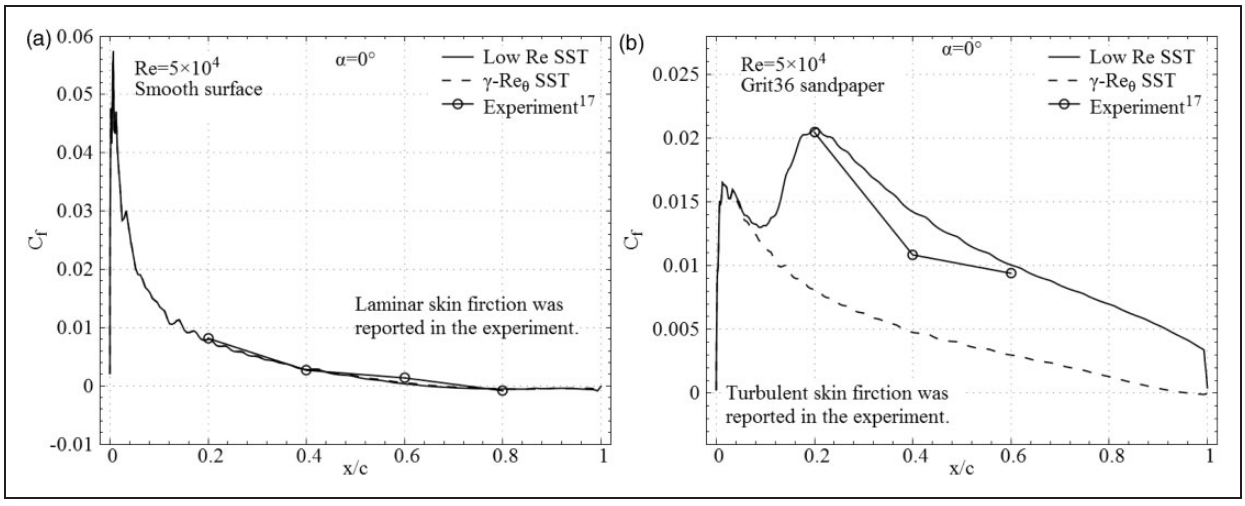

Figure 5. C_f comparisons on the Grit-36 upper surface.
SST: shear stress transport.

separation zone, as can be observed in Figure 5(a) and (b). Although the experimental drag coefficients are not available at this Reynolds number for exact comparisons, the prediction in the trend of drag variation is obviously wrong for the γ-Re_θ SST model at $Re = 5 \times 10^4$.

Flow field result at $Re = 1.5 \times 10^5$

Figure 6 and Figure 7 show the flow field at a representative $\alpha = 6°$, accompanied with the pressure and skin friction results. The normalised Reynolds shear stress is compared to facilitate understanding.

Table 4. Drag coefficients comparison at $Re = 5 \times 10^4$.

	Smooth		Grit-36	
	Low Re SST	γ-Re_θ SST	Low Re SST	γ-Re_θ SST
C_{dp}	0.01018	0.01033	0.00645	0.00497
C_{df}	0.00942	0.00957	0.02361	0.00978
C_d	0.01960	0.01989	0.03006	0.01475

For the smooth aerofoil, Figure 6 shows that, both models predict a transitional leading edge separation bubble on the upper surface. The prediction of the two models is generally similar. The bubble location is 0.05 c-0.23 c and 0.06 c-0.23 c for the γ-Re_θ SST model and the low Re SST model, respectively. The Reynolds shear stress exceeds the cut-off level 0.001 at 0.16 c for both models. Figure 6(c) and (d) show clear differences in pressure and skin friction distribution in the bubble area, but they are similar, leading to little differences in the total lift and drag coefficients.

On the Grit-36 rough surface, both predict no separation bubbles on the upper surface, as shown in Figure 7(a) and (b). The Reynolds shear stresses show that the low Re SST model predicts turbulent boundary layer starting from the leading edge as confirmed by the skin friction results in Figure 7(d). The Reynolds shear stress predicted by the γ-Re_θ SST model exceeds the threshold at 0.41 c above the upper surface. This in some degree agrees with the skin friction data, taking the minimum skin friction as the transition onset location (0.46 c). The γ-Re_θ SST model's prediction of later transition on the upper surface and lack of transition on the lower

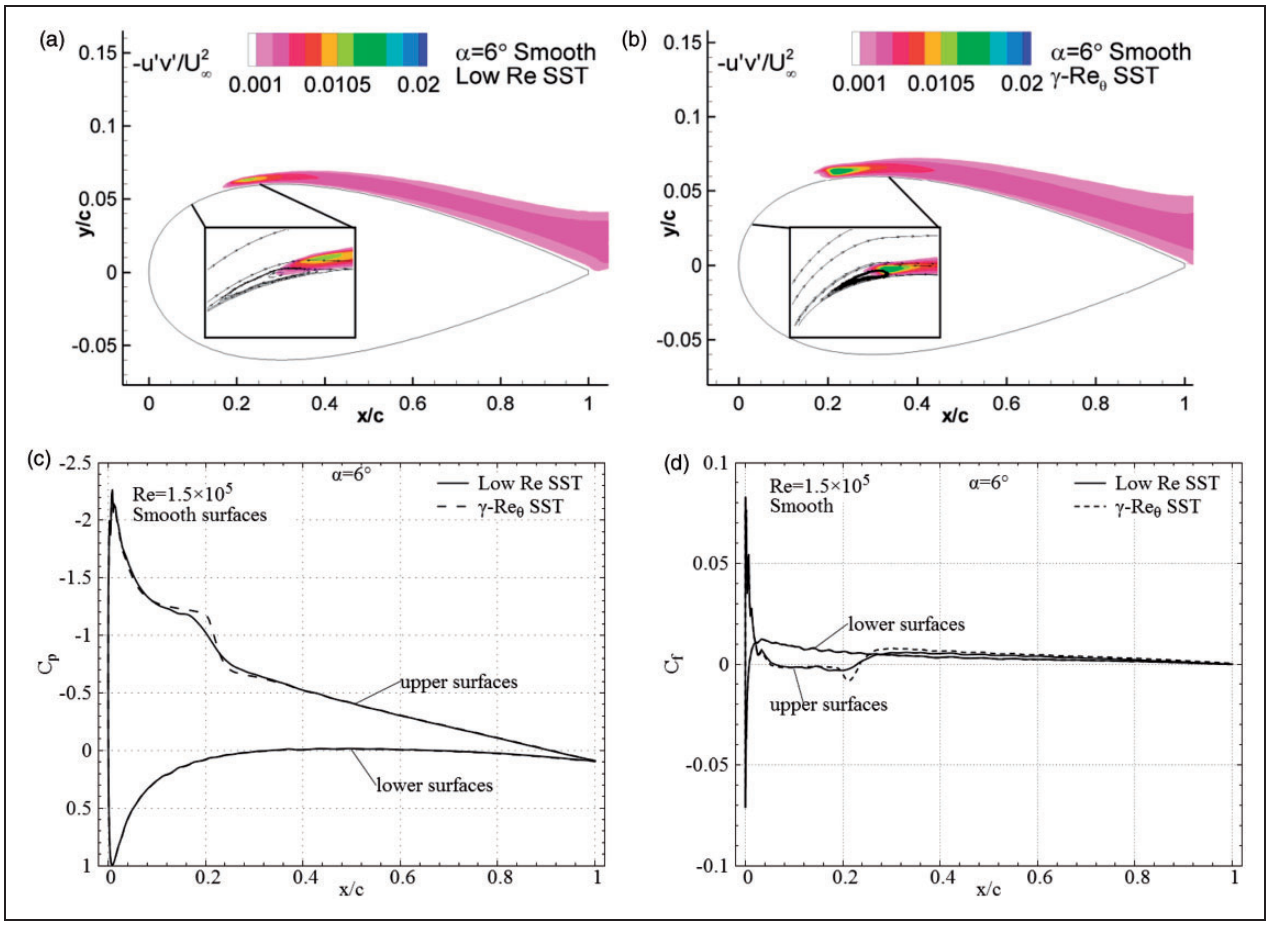

Figure 6. Flow field, pressure, and skin friction results (x to y scale is 0.3 in (a) and (b)).
SST: shear stress transport.

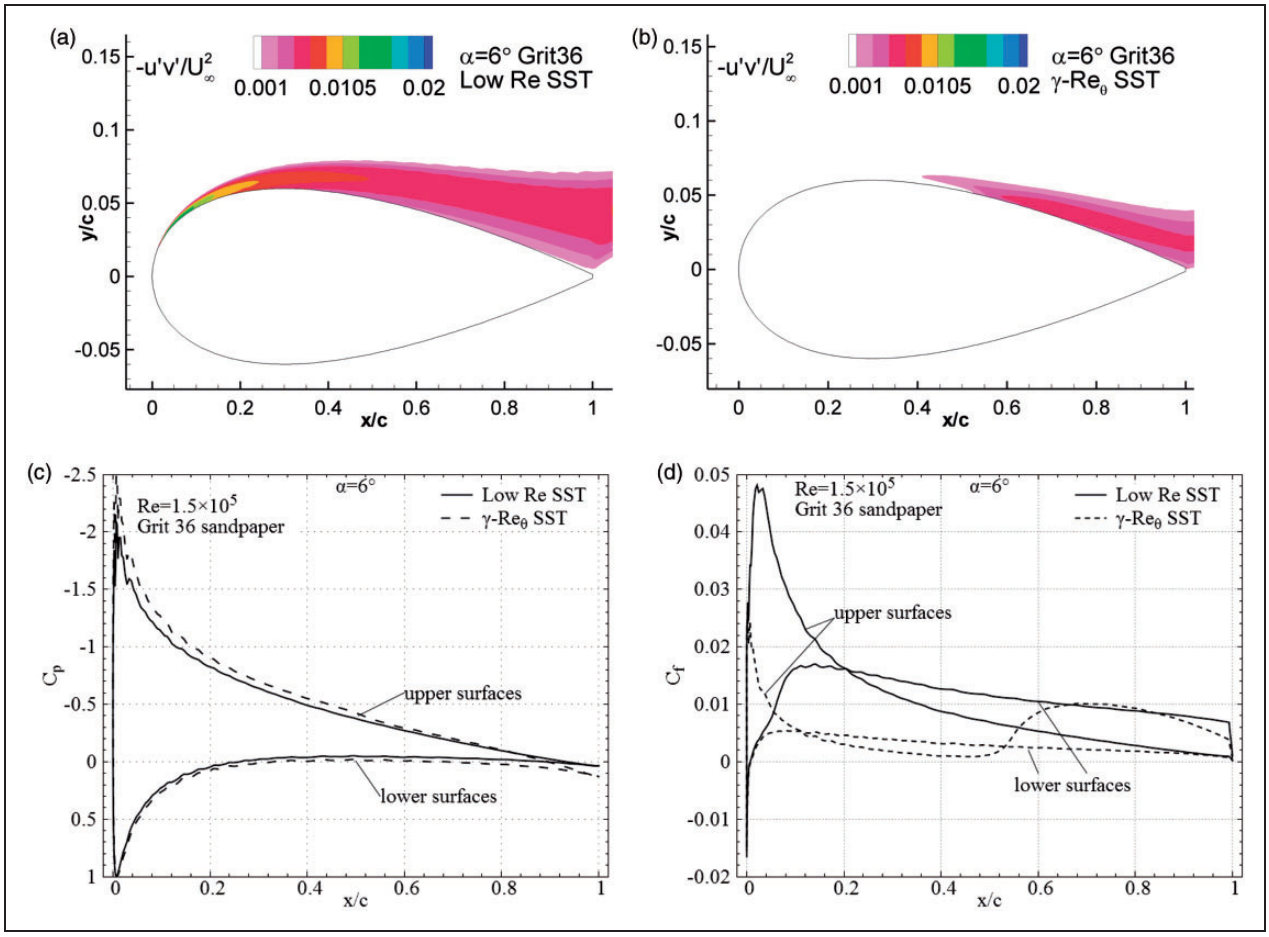

Figure 7. Flow field, pressure, and skin friction results (*x* to *y* scale is 0.3 in (a) and (b)).
SST: shear stress transport.

surface result in much lower skin friction, as shown in Figure 7(d). Obviously, the skin friction magnitude in Figure 7(d) is directly related to the Reynolds shear stresses in Figure 7(a) and (b).

The difference in the drag coefficient predicted by the two models is largely attributed to the difference in the skin friction due to different boundary layer status. Additionally, on the upper surface, the γ-Re_θ SST model increases the peak of the pressure coefficient, as shown in Figure 7(c). This explains the increase of the lift coefficient in Figure 4(a), inconsistent with the experimental trend.

Further discussion

The two models predict transition in different ways. In the case of low Re SST model, the point where the production of turbulent kinetic energy overtaking the dissipation is defined as the transition onset and the point where the 'near balance is achieved' between the production and the dissipation is defined as the point when the boundary layer becomes fully turbulent. When roughness induced transition is considered, the boundary condition for ω and some model coefficients are changed, according to rough surface experimental data. The increase of the roughness height will decrease the ω wall value and then decrease the dissipation term in the k transport equation, resulting earlier transition to occur.[34]

In the case of γ-Re_θ SST model, an empirical correlation for transition onset and completion is used. Local critical Reynolds number is calculated through the correlation based on the geometrical roughness height, turbulence intensity and pressure gradient. As mentioned earlier, the correlation was developed for relatively high turbulence intensities (>1%), and it may not perform well in the low incoming flow intensity as in current cases (<0.5%). This shortcoming may be one source of the problem attributing to the difficulty of the model for rough surface transition prediction.

Conclusion

By using the equivalent sand grain approach in RANS simulation for a rough surface aerofoil, this paper investigates the roughness modelling of the γ-Re_θ SST model and the low Reynolds number SST model for low Reynolds number transitional flows. The primary observed roughness effect is the decrease in lift, increase in drag, increase in skin friction and roughness induced transition in boundary layers for

the NACA0012 aerofoil at $Re = 1.5 \times 10^5$. The results on smooth surfaces from both models show similar skin friction, pressure and lift and drag predictions. The results on rough surfaces show that the low Re SST model is capable of modelling the roughness effects in a consistent way as compared with the experiment. The γ-Re_θ SST model, on the other hand, fails to give an effective prediction for transitional flow on rough surfaces, resulting in incorrect lift and drag predictions.

Funding

This research received no specific grant from any funding agency in the public, commercial, or not-for-profit sectors.

Conflict of interest

None declared.

Acknowledgements

We acknowledge Luís Eça for fruitful discussions. Hemant Punekar and Balasubramanyam Sasanapuri from ANSYS Technical Support are also acknowledged for information on the implementation of the γ-Re_θ SST model and the related roughness model.

References

1. Schmitz FW. *Aerodynamics of the model airplane, part 1: Airfoil measurements*. NASA-TM-X-60976, 1967.
2. Kraemer K. *Airfoil profiles in a critical Reynolds number region*. NASA-TT-F-14959, 1973. Translation of 'Flügelprofile im kritischen Reynoldszahl Bereich,' *Zeitschrift Forschung auf dem Gebiete des Ingenieurwesens* 1961; 27(2): 33–46.
3. Lyon CA, Broeren AP, Giguère P, et al. *Summary of low-speed airfoil data*. vol. 3, Virginia Beach, VA: SoarTech Publications, 1998, pp.102–105, 107–109, 164–187.
4. Althaus D. *Profilpolaren für den Modellflug: Windkanalmessungen an Profilen im kritischen Reynoldszahlbereich, Band 2*. Villingen, Germany: Neckar-Verlag VS, 1985, pp.32–36, 154–168.
5. Simons M. *Model aircraft aerodynamics*. 4th ed. Dorset, UK: Special Interest Model Books, Ltd, 1999, p.99, 125–126, 240.
6. Gopalarathnam A, Broughton BA, Mcgranahan BD, et al. Design of low Reynolds number airfoils with trips. *J Aircraft* 2003; 40(4): 768–775.
7. Zhou Y and Wang ZJ. Effects of surface roughness on separated and transitional flows over a wing. *AIAA J* 2012; 50(3): 593–609.
8. Huebsch WW, Gall PD and Hamburg SD. Dynamic roughness as a means of leading-edge separation flow control. *J Aircraft* 2012; 49(1): 108–115.
9. Nikuradse J. *Law of flow in rough pipes*. NACA TM-1292, 1950. Translation of 'Strömungsgesetze in rauhen Rohren', VDI-Forschungsheft 361, Beilage zu 'Forschung auf dem Gebiete des Ingenieurwesens' Ausgabe B Band 4, July/August 1933.
10. Eça L and Hoekstra M. Numerical aspects of including wall roughness effects in the SST k–ω eddy-viscosity turbulence model. *Comput Fluids* 2011; 40(1): 299–314.
11. Dirling RB. A method for computing roughwall heat transfer rates on reentry nosetips. In: *AIAA 8th thermophysics conference*, Palm Springs, CA, USA, pp.73–763. AIAA.
12. Feindt EG. *Untersuchungen über die Abhängigkeit des Umschlages laminar- turbulent von der Oberflächenrauhigkeit und der Druckverteilung*. Dissertation Brauschweig, 1956, also see Schlichting H. *Boundary layer thoery*. 7th ed. New York: McGraw-Hill, 1979, pp.540–542.
13. Stripf M, Schulz A, Bauer H-J, et al. Extended models for transitional rough wall boundary layers with heat transfer—Part I: Model formulations. *J Turbomachinery* 2009; 131(3): 31016.
14. Elsner W and Warzecha P. Modelling of rough wall boundary layers with an intermittency transport model. *TASK Quart* 2010; 14(3): 271–282.
15. Dassler P, Kožulović D and Fiala A. Transport equation for roughness effects on laminar – turbulent transition. In: *The 15th international conference on fluid flow technologies, conference on modelling fluid flow (CMFF' 12)*, Budapest University of Technology and Economics, Budapest, Hungary, 2012.
16. Chen ZJ, Qin N and Nowakowski AF. Three-dimensional laminar-separation bubble on a cambered thin wing at low Reynolds numbers. *J Aircraft* 2012; 50(1): 152–163.
17. Chakroun W, Al-Mesri I and Al-Fahad S. Effect of surface roughness on the aerodynamic characteristics of a symmetrical airfoil. *Wind Eng* 2004; 28(5): 547–564.
18. Chakroun WM, Abdel-Rahman AA and Taylor RP. Effect of surface roughness on flow over a circular cylinder and flapped airfoil. In: *ASME fluids engineering division conference*, San Diego, California, USA, FED-Vol. 237, 1996, pp.845–853.
19. Ferrer E and Munduate X. CFD predictions of transition and distributed roughness over a wind turbine airfoil. In: *47th AIAA aerospace sciences meeting including the new horizons forum and aerospace exposition*, AIAA Paper 2009-269, 2009.
20. Pailhas G, Touvet Y and Aupoix B. Effects of Reynolds number and adverse pressure gradient on a turbulent boundary layer developing on a rough surface. *J Turbulence* 2008; 9(43): 1–24.
21. Menter FR. Two-equation eddy-viscosity turbulence models for engineering applications. *AIAA J* 1994; 32(8): 1598–1605.
22. Menter FR, Kuntz M and Langtry R. Ten years of industrial experience with the SST turbulence model. In: K Hanjalic, Y Nagano and M Tummers (eds) *Turbulence heat and mass transfer 4*. Redding, CN: Begell House, Inc, 2003, pp.625–632.
23. ANSYS® FLUENT. *Academic research, Release 14.0, ANSYS FLUENT theory guide*. Canonsburg, PA: ANSYS, Inc, 2011, p.84.
24. Langtry RB and Menter FR. Correlation-based transition modelling for unstructured parallelized computational fluid dynamics codes. *AIAA J* 2009; 47(12): 2894–2906.
25. Langtry R and Menter F. *Overview of industrial transition modelling in CFX*. ANSYS Germany, ANSYS CFX, 2006, pp.63–65, 67–72, 129–133.

26. Mayle RE. The 1991 IGTI scholar lecture: The role of laminar-turbulent transition in gas turbine engines. *J Turbomachinery* 1991; 113(4): 509–536.
27. Pimenta MM, Moffat RJ and Kays WM. *The turbulent boundary layer: An experimental study of the transport of momentum and heat with the effect of roughness*. Report HMT-21, The Office of Naval Research, USA, 1975.
28. Stripf M, Schulz A and Wittig S. Surface roughness effects on external heat transfer of a HP turbine vane. *J Turbomachinery* 2005; 127(1): 200–208.
29. Hellsten A and Laine S. Extension of k–ω shear-stress transport turbulence model for rough-wall flows. *AIAA J* 1998; 36(9): 1728–1729.
30. Menter F, Ferreira JC, Esch T, et al. The SST turbulence model with improved wall treatment for heat transfer predictions in gas turbines. In: *Proceedings of the international gas turbine congress*, IGTC2003-TS-059, Gas Turbine Society of Japan, Tokyo, 2003, pp.1–7.
31. Ioselevich VA and Pilipenko VN. Logarithmic velocity profiles for Flow of a weak polymer solution near a rough surface. *Soviet Phys Dokl* 1974; 18: 790–796.
32. Menter FR, Langtry RB, Likki SR, et al. A correlation-based transition model using local variables—part I: Model formulation. *J Turbomachinery* 2006; 128(3): 413–422.
33. Roache PJ. *Fundamentals of verification and validation*. 2nd ed. Socorro, NM: Hermosa Publications, 2009, pp.450–452.
34. Wilcox DC. *Turbulence modelling for CFD*. 3rd ed. La Cãnada, CA: DCW Industries, 2006, p.216.

Appendix

Notation

c	aerofoil chord length
C_l	lift coefficient, $C_l = L/(0.5\rho U_\infty^2 S_{ref})$
C_d	drag coefficient, $C_d = D/(0.5\rho U_\infty^2 S_{ref})$
C_f	local skin friction coefficient
h	roughness height
h^+	nondimensional roughness height, $h^+ = \rho u_\tau h/\mu$
$\overline{h}$	average roughness height
k	turbulent kinetic energy in k – ω model
Re	Reynolds number, $Re = \rho U_\infty L_{ref}/\mu$
T	temperature
Tu	turbulence intensity, %
u_τ	friction velocity, $u_\tau = \sqrt{\tau_w/\rho}$
$-u'v'/U_\infty^2$	normalised Reynolds shear stress
x	position in x-coordinate
y	cell wall distance
y^+	nondimensional cell wall distance, $y^+ = \rho u_\tau y/\mu$
α	angle of attack
α_1, α^*, α^*_∞, α^*_0	model coefficients of the low Re SST model
μ	viscosity
μ_t	turbulent viscosity (eddy viscosity)
μ_t/μ	viscosity ratio
ω	specific dissipation rate in k-ω model
ρ	air density
τ_w	wall shear stress

Subscripts

g	geometrical
inlet	values at inlet
ref	reference values
s	sand grain
∞	freestream
θ	momentum thickness